Supplementary file for Synergistic Interactions in $LaMnO_3$/CuO Composites with Enhanced Supercapacitive Performance

Alisha Dhakal[a†], Felio R Perez[b], Shawn David Pollard[a], Sanjay R. Mishra[a†]
[a] Department of Physics and Materials Science, The University of Memphis, Memphis, Tennessee 38152, United States.
[b] Integrated Microscopy Center, The University of Memphis, Memphis, Tennessee 38152, United States.

Content

Figure S1: The elementary mapping of O (red), La (blue), Mn (green), and Cu (magenta) of LMO/CuO composites.
Table S1: Specific surface area and pore size distribution of LMO/CuO composites.
Figure S2: Relation between **(a)** log current and log scan rate of LMO/CuO composites, **(b)** peak current of CV curves and square root of scan rate, and **(c)** capacitive/diffusion contribution with scan rate from 1 to 200 mV/s.
Figure S3: (**a, c, e**, and **g**) CV curves at different scan rates and (**b, d, f,** and **h**) charge/discharge curves at different current densities of the electrode based on LMO/CuO composites with molar ratio 1:0, 0:1, 7:3, and 1:1, respectively.
Table S2: Specific capacitance, energy density, and power density of LMO/CuO composites.
Table S3: Equivalent fitting values of the Nyquist plot of LMO/CuO composites.
Table S4: Electrochemical performance metrics of $LaMnO_3$ and CuO-based electrode materials for energy storage devices.
Table S5: Equivalent fitting values of the Nyquist plot of LMO/CuO composites after stability test.
Figure S4: (a-h) FESEM images of LMO/CuO composites coated on Ni-foam before and after the stability test.

Keywords: $LaMnO_3$ and CuO composites; Electrochemical analysis; Autocombustion; Supercapacitors; Energy Storage

† Corresponding author: srmishra@memphis.edu (S. R. Mishra)
adhakal@memphis.edu (A. Dhakal)

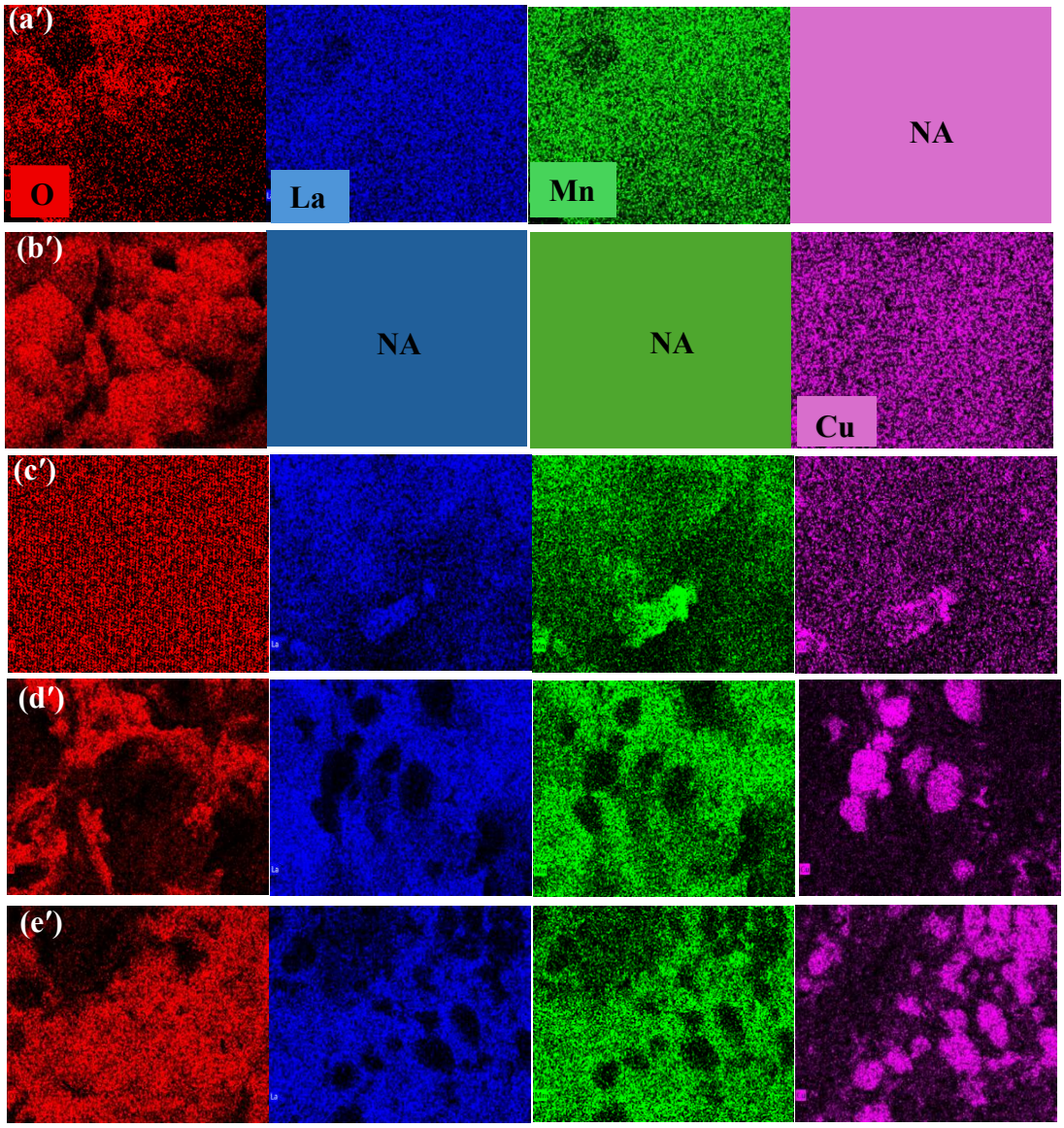

Figure S1: The elementary mapping of O (red), La (blue), Mn (green), and Cu (magenta) of LMO/CuO composites.

Table S1: Crystallite size, Specific surface area and pore size distribution of LMO/CuO composites.

Composites	Crystallite size (nm)		BET surface area (m^2g^{-1})	Average pore size (radius nm)	Total Pore Volume (ccg^{-1})
	$LaMnO_3$	CuO			
LMO/CuO(1:0)	35.4	-	3.917	4.359	0.009
LMO/CuO(0:1)	-	19.6	0.124	15.121	0.001
LMO/CuO(9:1)	31.5	16.1	13.826	2.118	0.015
LMO/CuO(7:3)	29.4	26.8	8.947	2.152	0.009

LMO/CuO(1:1)	28.7	28.3	4.173	1.793	0.004

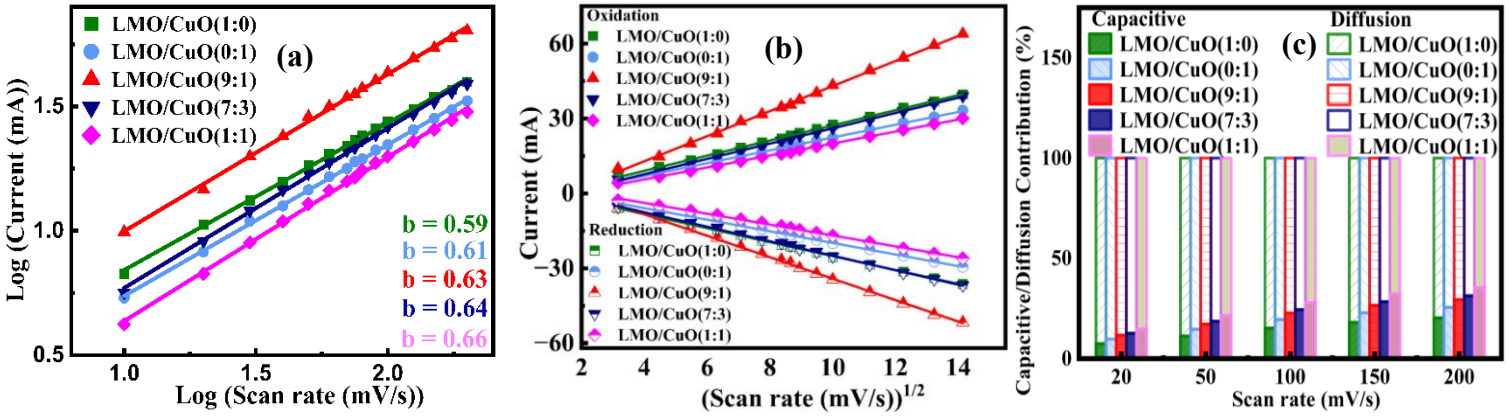

Figure S2: Relation between **(a)** log current and log scan rate of LMO/CuO composites, **(b)** peak current of CV curves and square root of scan rate, and **(c)** capacitive/diffusion contribution with scan rate from 1 to 200 mV/s.

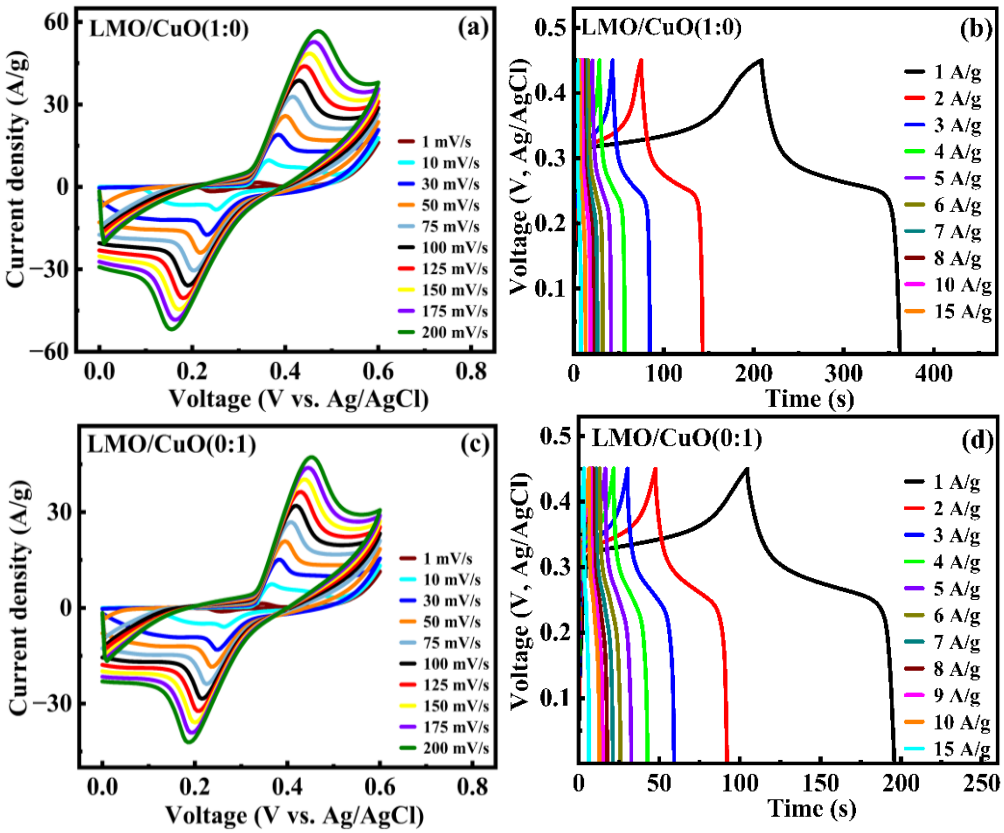

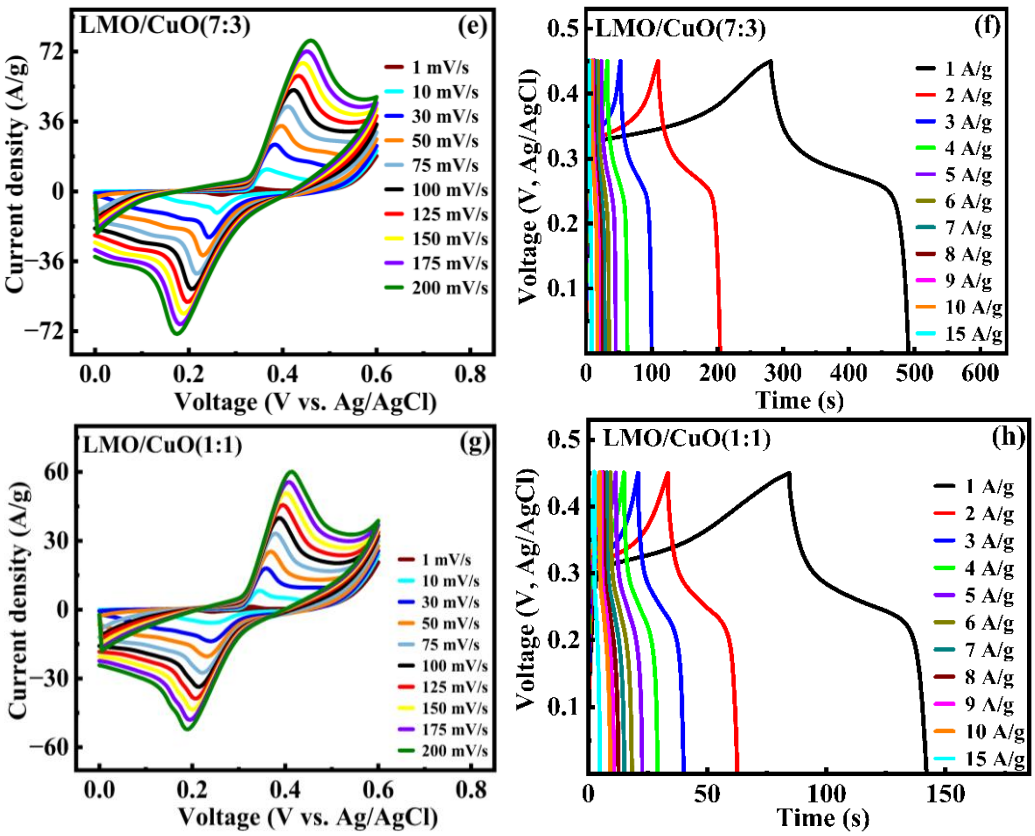

Figure S3: (**a, c, e**, and **g**) CV curves at different scan rates and (**b, d, f,** and **h**) charge/discharge curves at different current densities of the electrode based on LMO/CuO composites with molar ratio 1:0, 0:1, 7:3, and 1:1, respectively.

Table S2: Specific capacitance, energy density, and power density of LMO/CuO composites.

Sample	C_{SP} (F/g)		Energy Density ($Whkg^{-1}$)	Power Density (Wkg^{-1})
	1 mVs^{-1}	1 Ag^{-1}		
LMO/CuO(1:0)	369.1	338.1	16.9	399.0
LMO/CuO(0:1)	284.4	202.7	10.1	399.2
LMO/CuO(9:1)	646.8	517.1	25.9	397.6
LMO/CuO(7:3)	430.1	465.2	23.3	397.7
LMO/CuO(1:1)	334.1	128.8	6.4	400.6

Table S3: Equivalent fitting values of the Nyquist plot of LMO/CuO composites.

Calcination Temperature (°C)	R_1 (Ω)	R_2 (Ω)	Wo, (Ω*10^{-3})	CPE_1 (α)	CPE_1) (Q; $Ω^{-1}s^{α}$)	CPE_2 (α)	CPE_2) (Q; $Ω^{-1}s^{α}$)	Goodness of Fit
LMO/CuO(1:0)	2.275	8.274	0.183	0.675	0.006	0.932	0.002	0.175
LMO/CuO(0:1)	2.425	8.540	0.068	0.739	0.003	0.950	0.002	0.102
LMO/CuO(9:1)	2. 211	6.353	0.134	0.686	0.007	0.946	0.002	0.152
LMO/CuO(7:3)	2.313	7.343	0.143	0.752	0.003	0.936	0.002	0.071
LMO/CuO(1:1)	2.325	8.790	0.101	0.751	0.004	0.950	0.002	0.112

Table S4 provides a comparison of the C_{SP}, energy density, and power density of the synthesized LMO composites with values reported in previously published studies. Based on this comparison, our composites demonstrate competitive performance and can be considered as promising electrode materials for achieving both high specific capacitance and power density.

Table S4: Electrochemical performance metrics of $LaMnO_3$ and CuO-based electrode materials for energy storage devices.

Material	Current Density or Scan Rate	Electrolyte (KOH)	C_{SP} (F/g)	Energy Density, E ($Whkg^{-1}$)	Power Density, P (Wkg^{-1})	Supplementary Referencees
LMO/CuO(9:1)	1 A/g	1 M	517.1	25.9	397.6	[**Present work**]
CeO_2-Fe_2O_3 nanospindles	5 mV/s	6 M	142.6	-	-	(1)
Porous NiO-CeO_2	1 A/g	3 M	305	-	-	(2)
$LaMnO_3$-Co_3O_4 (70%:30%)	0.5 A/g	1 M	660.0	33.0	202.7	(3)
Co-CeO_2	2 A/g	1 M	573 C/g	-	-	(4)
$La_{0.75}Sr_{0.25}MnO_{3-\delta}$ /MnO_2	2 mV/s	1M Na_2SO_4	437.2	-	-	(5)
CeO_2/CeS_2	1 A/g	0.1 M	420	21.2	303.0	(6)
$LaMnO_3$-CeO_2 (70%:30%)	1 A/g	1 M	637.6	31.9	357.5	**(7)**
MnO_2-CeO_2-1	0.5 A/g	3 M	274.3	-	-	(8)

Table S5: Equivalent fitting values of the Nyquist plot of LMO/CuO composites after stability test.

Calcination Temperature (°C)	R_1 (Ω)	R_2 (Ω)	Wo, (Ω*10^{-3})	CPE_1 (α)	CPE_1) (Q; $Ω^{-1}s^{α}$)	CPE_2 (α)	CPE_2) (Q; $Ω^{-1}s^{α}$)	Goodness of Fit
LMO/CuO(1:0)	2.275	9.654	0.230	0.663	0.007	0.957	0.002	0.686
LMO/CuO(0:1)	2.322	13.898	0.294	0.656	0.008	0.965	0.003	0.993
LMO/CuO(9:1)	2.320	7.253	0.007	0.748	0.003	0.938	0.002	0.007
LMO/CuO(7:3)	2.424	9.158	0.093	0.732	0.004	0.9596	0.002	0.453
LMO/CuO(1:1)	2.225	10.606	0.185	0.718	0.004	0.924	0.003	0.558

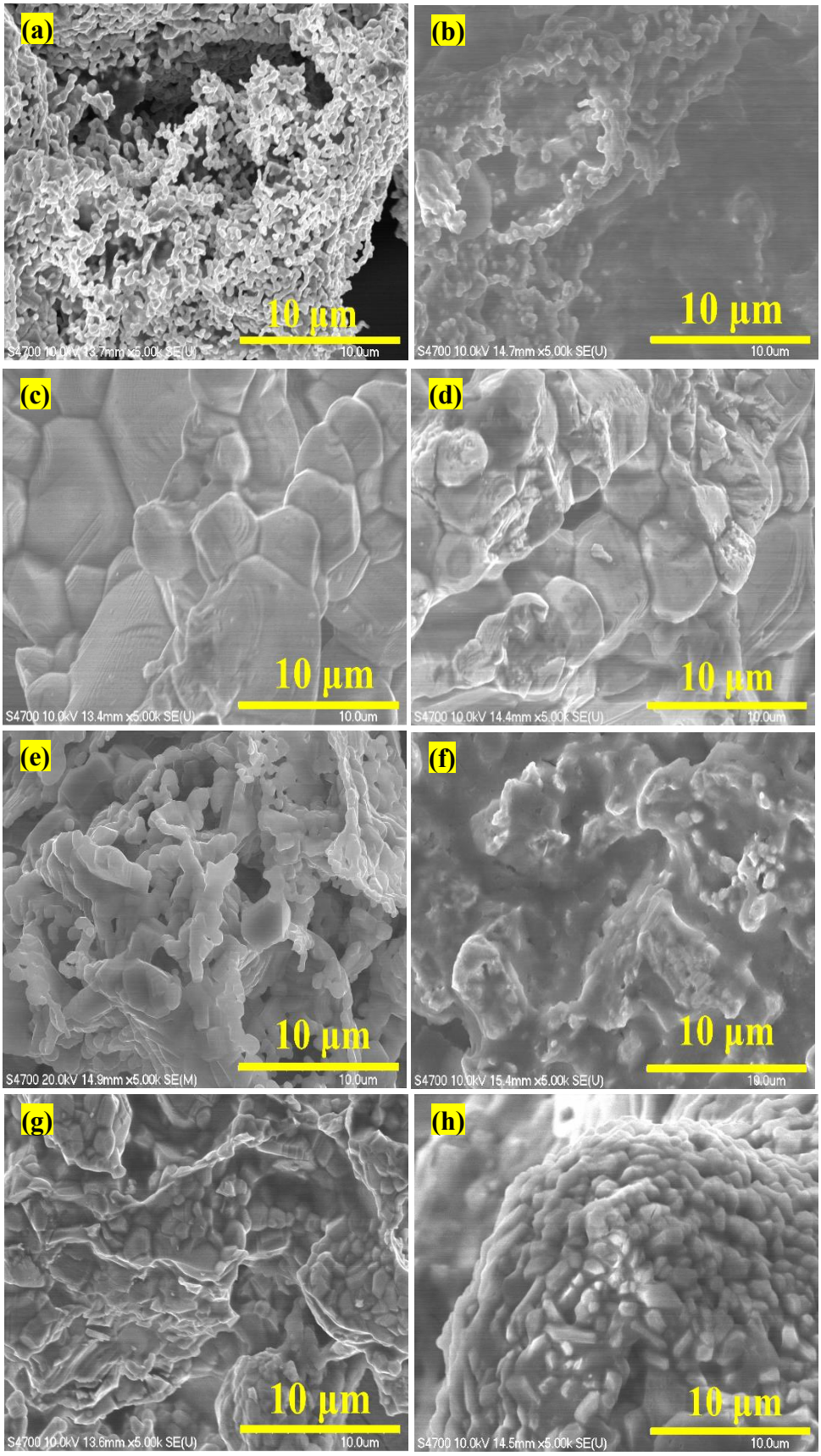
(a)
10 µm
(b)
10 µm
S4700 10.0kV 14.7mm x5.00k SE(U)
10.0um
(c)
10 µm
S4700 10.0kV 13.4mm x5.00k SE(U)
10.0um
(d)
10 µm
S4700 10.0kV 14.4mm x5.00k SE(U)
10.0um
(e)
10 µm
S4700 20.0kV 14.9mm x5.00k SE(M)
10.0um
(f)
10 µm
S4700 10.0kV 15.4mm x5.00k SE(U)
10.0um
(g)
10 µm
S4700 10.0kV 13.6mm x5.00k SE(U)
10.0um
(h)
10 µm
S4700 10.0kV 14.5mm x5.00k SE(U)
10.0um

Figure S4: (a-h) FESEM images of LMO/CuO composites coated on Ni-foam before and after the stability test.

Supplementary References

1. Arul NS, Mangalaraj D, Ramachandran R, Grace AN, Han JI. Fabrication of CeO_2/Fe_2O_3 composite nanospindles for enhanced visible light driven photocatalysts and supercapacitor electrodes. J Mater Chem A Mater. 3:15248–58.
2. Padmanathan N, Selladurai S. Electrochemical capacitance of porous NiO–CeO_2 binary oxide synthesized via sol–gel technique for supercapacitor. Ionics (Kiel). 20:409–20.
3. Dhakal A, Mishra SR, Perez F. Synergetic Effect Towards High Electrochemical Performance in $LaMnO_3$-Co_3O_4 Composites. Energy Advances;
4. Murugan R, Ravi G, Yuvakkumar R, Rajendran S, Maheswari N, Muralidharan G, et al. Pure and Co doped CeO_2 nanostructure electrodes with enhanced electrochemical performance for energy storage applications. Ceram Int. 43:10494–501.
5. Lv J, Zhang Y, Lv Z, Huang X, Wang Z, Zhu X, et al. Strontium doped lanthanum manganite/manganese dioxide composite electrode for supercapacitor with enhanced rate capability. Electrochim Acta. 222:1585–91.
6. Bibi N, Xia Y, Ahmed S, Zhu Y, Zhang S, Iqbal A. Highly stable mesoporous CeO_2/CeS_2 nanocomposite as electrode material with improved supercapacitor electrochemical performance. Ceram Int. 44:22262–70.
7. Dhakal A, Perez F, Mishra SR. Unveiling the Synergistic Potential of $LaMnO_3$-CeO_2 Composites in Supercapacitor Applications. RSC Sustainability;
8. Zhang H, Gu J, Tong J, Hu Y, Guan B, Hu B, et al. Hierarchical porous MnO_2/CeO_2 with high performance for supercapacitor electrodes. Chemical Engineering Journal. 286:139–49.